Focussed on: Fracture and Structural Integrity related Issues

Investigation of very high cycle fatigue by thermographyc method

V. Crupi, G. Epasto, E. Guglielmino, G. Risitano
University of Messina, Department of Electronic Engineering, Chemistry and Industrial Engineering (DIECII)
crupi.vincenzo@unime.it; gabriella.epasto@unime.it; eguglie@unime.it; grisitano@unime.it

ABSTRACT. Nowadays, many components and structures are subjected to fatigue loading with a number of cycles higher than 10^7. In this scientific work, the behaviour of two kinds of tool steel was investigated in very high cycle fatigue regime. The fatigue tests were carried out at the frequency of 20 kHz and in fully reversed tension-compression mode (R = -1) by means of an ultrasonic fatigue testing equipment. The radiometric surface temperature was detected during all the test by means of an IR camera in order to extend the Thermographic Method and the Energetic Approach in very high cycle fatigue regime. The failure mechanism of the investigated steels was evaluated by means of several experimental techniques (scanning electron microscopy, Energy Dispersive X-ray spectroscopy and Optical Microscopy).

KEYWORDS. Very High Cycle Fatigue; Thermographic method; Energetic approach; Failure analysis; Microscopy.

INTRODUCTION

With the increasing progress of the technological development in structural applications of tool steels, the required fatigue life has increased, so it is very important to determine a safe fatigue strength for 10^9 cycles. Nowadays, the very high cycle fatigue (VHCF) constitutes one of the main fatigue design criteria.

Many researches published important scientific works based on the results of ultrasonic fatigue testing. In 1999 Bathias [1] experimentally proved that there is no infinite life in metallic materials and in 2007 Sonsino [2] showed that a continuous decrease of fatigue strength occurs in the range of large cycle numbers.

The fatigue crack initiation in the gigacycle regime seems to occur essentially inside the specimen [1] and not at the surface as it generally occurs in the low cycle fatigue (LCF) and high cycle fatigue (HCF) regime. This means that the effect of environment is quite small in the gigacycle regime as the initiation of short cracks is inside the specimen and the surface plays a minor role especially if it is smooth. The effect of internal hydrogen trapped by non-metallic inclusions on high cycle fatigue was first indicated by Murakami et al. [3]. They observed that around the internal inclusion, from which the failure starts, an optical dark area (ODA) can be seen by an optical microscope. The rule of a crack initiation located inside the specimen in VHCF regime is not rigid, but has several exceptions. According to Bayraktar et al. [4], the crack initiation site in some automotive metallic alloys is not always in the interior of the specimen. Moreover, the cause of the initiation site can be not only inclusions, but also the pores. Sohar et al. [5] carried out ultrasonic fatigue testing on AISI D2 type wrought cold work tool steel, finding that crack growth behaviour can follow two mechanisms: the so-called fisheye (internal crack initiation) or half-of fish-eye (near-surface crack initiation), depending to the presence of primary carbides (clusters).

Moreover the temperature evolution during the fatigue tests in HCF [6 - 10] and LCF [11] regimes has been investigated by several researchers, but there are only few studies in VHCF regime. Xue et al. [12] investigated fatigue damage

progression of three kinds of alloy in the VHCF regime by thermographic analysis. Blanche et al. [13] proposed a heat diffusion model to estimate dissipated energy during VHCF tests at high loading frequency (20 kHz) and low stress.
The authors of the present paper have a strong background in the infrared thermography (IRT), which was proved to be effective in obtaining results in several fields: correlation between the values of stabilization of the temperature increments and the areas of the thermal hysteresis loops in LCF [11], fatigue assessment of mechanical components [14], relationship between the temperature evolution and the internal microstructural changes [15], correlation between internal damping and the temperature increment of metals subjected to fatigue loading [16], damage cumulative evaluation [17], analysis of sandwiches under impact loading [18].
In the present paper, the infrared (IR) thermography and an energetic approach were applied to investigate and compare a cold work tool steel (DIN EN 115CrV3) and a free-cutting steel (DIN EN 60SPb20+Bi) in VHCF range. Moreover, the failure mechanism was evaluated by means of several experimental techniques (scanning electron microscopy, Energy Dispersive X-ray spectroscopy and Optical Microscopy). The aim of the failure analysis was to assess if the nature of the microstructure and the metallurgical defects, in terms of inclusions and pores, can influence the crack initiation.

MATERIAL AND METHODS

The fatigue tests were performed without cooling at R= -1 and f= 20 kHz by a piezoelectric fatigue machine (Fig. 1a). The vibration of the specimen is included with a piezo-ceramic transducer, which generates acoustical waves to the specimen through a power concentrator (horn). The specimen geometry is represented in Fig. 1b. The dynamic displacement amplitude of the specimen extremity is controlled in order to keep constant the stress during the test, through the computer control. The test is automatically stopped when the frequency falls down to 19.5 kHz.
The tests were carried out on specimens made of a high carbon cold work tool steel (DIN EN 115CrV3) and an unalloyed free-cutting high carbon steel with lead (DIN EN 60SPb20+Bi). The chemical composition of the investigated specimens was derived from X-ray fluorescence analysis and the results are shown in Tab. 1.

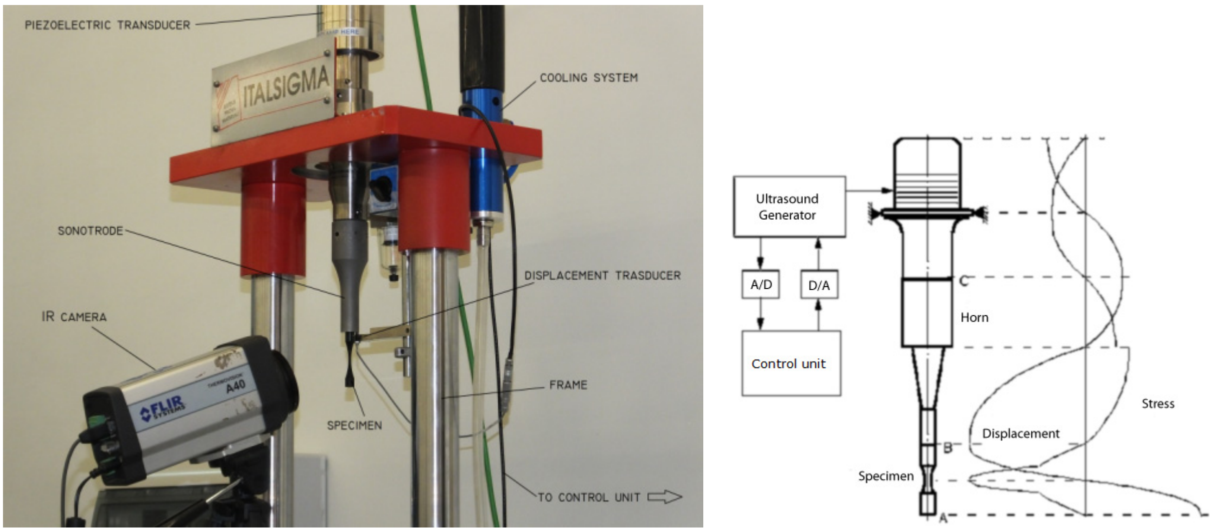

(a)

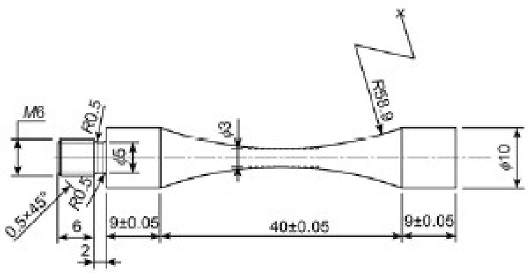

(b)

Figure 1: (a) Experimental set-up and (b) geometry of the specimens (units: mm).

Grade			DIN/EN				Grade			DIN/EN			
1.2210			115CrV3				1.0758			60SPb20+Bi			
Si %	Mn %	S %	Cr %	V %	Pb %	Fe %	Si %	Mn %	S %	Cr %	Mo %	Pb %	Fe %
0.22	0.34	0.027	0.69	0.09	-	balance	0.25	1.34	0.39	0.24	0.024	0.27	balance

Table 1: Chemical composition of the tested specimens by means of XRF analysis.

During the fatigue tests, the radiometric surface temperature was measured by an uncooled long wave infrared (LWIR) focal plane array camera with a resolution of 320x240 pixels and a measurement accuracy of ± 2 °C (model FLIR Systems A40M). The frame rate during the acquisition of thermal increment was of one frame per minute.
Moreover, fractographies were carried out by means of a scanning electron microscope (SEM – JEOL JSM5900LV) and an optical stereomicroscope (SM – Leica M165C).

RESULTS AND DISCUSSION

S-N curve

The experimental results, obtained by the fatigue tests, are shown in fig. 2 in semi-logarithmic scale. According to the multistage fatigue life diagram [19, 20], the fatigue life diagram of 115CrV3 can be divided into four regions.
Unlike the material 115CrV3, the material 60SPb20+Bi presents a different behaviour with a continuous decrease of the fatigue life. The S-N curve has not the same slope, which has a significant decrease at a number of cycles equal to about 10^7, the slope decreases.

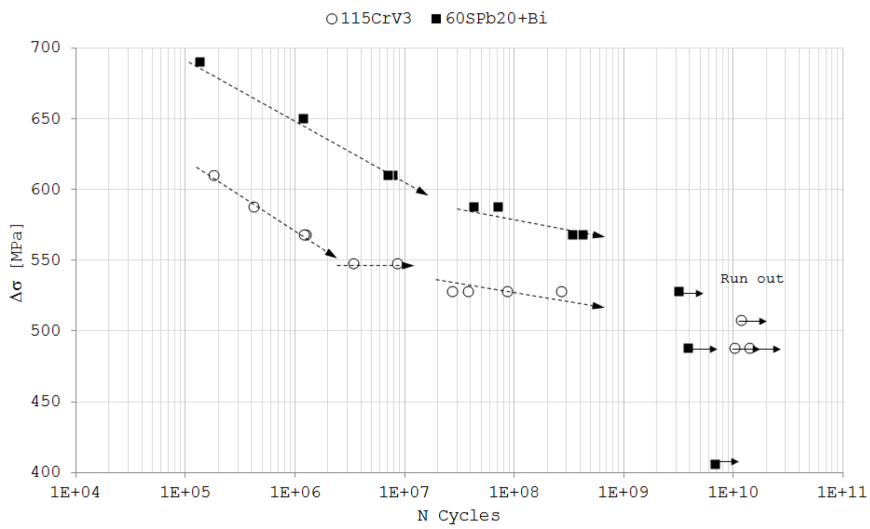

Figure 2: Fatigue life diagrams.

Energetic approaches

During HCF tests of common engineering metals and welded joints [6 - 10], the temperature evolution of the specimen, detected by means of an infrared camera, undergoes three separate phases. When a specimen is cyclically loaded above its fatigue limit, its superficial temperature usually rises quickly in the initial phase (phase 1), then reaches a stabilised asymptotic value (phase 2), and eventually this asymptote is left when plastic deformations become quite important, leading soon to failure after few cycles, with a very high further temperature increment (phase 3). The same trend was observed in LCF regime by Crupi et al. [11]. This temperature evolution is closely related to the internal microstructural changes, as demonstrated in [15], and to crack initiation and propagation [21].
In the present study, the temperature evolution in VHCF regime was analysed using an IR thermography. The $\Delta T_d - N$, obtained applying the IR thermography in VHCF regime, shows a similar trend with the three stages.

Crupi [16] developed a theoretical model able to describe the temperature evolution during the phases 1 and 2 of the fatigue life:

$$\Delta T_d = \Delta T_{as} \cdot \left(1 - e^{-\frac{N}{\tau}}\right) \tag{1}$$

where τ is a constant; if N is τ then ΔT_d is 0,63 ΔT_{as} and if N is 4τ then ΔT_d is 0,98 ΔT_{as}. The value of 4τ, applied successfully to conventional steel under HCF loading in [16], was considered also in the investigated VHCF tests. The ΔT_d - N data were interpolated by means of an exponential function according to eq. (1) and the convergence was achieved, as demonstrated in fig. 3 for 115CrV3 and for 60SPb20+Bi. As can be seen, for both materials there is a strong correlation between the experimental data and the theoretical ones.

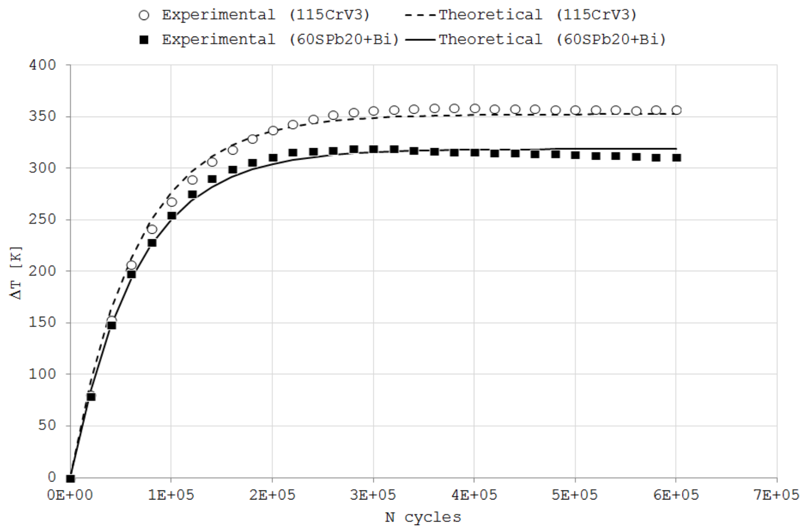

Figure 3: Experimental and theoretical ΔT_d - N curves.

Fig. 4 shows the values of asymptotic temperature increment during fatigue test ΔT_{as} (phase 2) as a function of the square of stress range applied $\Delta\sigma^2$ for the two investigated steels: 115CrV3 and 60SPb20+Bi. The behaviour of the 60SPb20+Bi is a confirmation of the linear trend in VHCF tests, the same already observed in the HCF tests [6, 14, 15, 16]. However, it is interesting to note that the 115CrV3 steel has a different trend, even if more tests should be necessary.

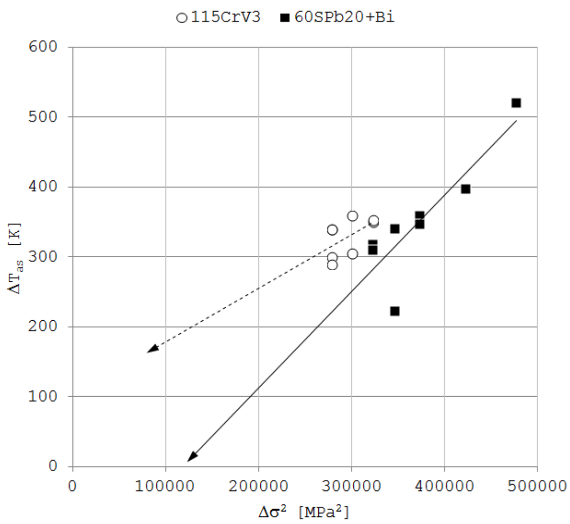

Figure 4: ΔT_{as} vs $\Delta\sigma^2$.

Energetic approaches, based on IR analysis, has been applied by several researchers [17, 22, 23, 24] in HCF regime to obtain the S-N curve and to assess the residual fatigue life. The basic assumption of the so-called "Energy Approach" [22] is that the fatigue failure takes place when the absorbed energy reaches a certain threshold value E_C characteristic for each structural detail. The limit energy E_C is proportional to the integral Φ of the ΔT_d - N curve:

$$E_C \propto \Phi = \int_0^{N_f} \Delta T_d(N)dN \tag{2}$$

where N_f is the number of cycles to failure. It has been ascertained that the energy absorbed by a unit volume of material till failure is the same when load histories at different levels are applied, so the energy parameter Φ is a material constant in HCF regime. The traditional Energetic Approach was developed by the authors in order to extend it in VHCF regime. The assessment of the integral Φ for the tests, carried out in a wide range of fatigue life, demonstrated that Φ is no longer constant for fatigue life higher than HCF zone (about $2 \cdot 10^6$), but increases by an order of magnitude with the increment of the number of cycles. Fig. 5 reports the trend of integral Φ as a function of $\Delta\sigma$ for both materials. It's possible to note that the value of the integral Φ of 115CrV3 decreases more steeply than the value of 60SPb20+Bi.

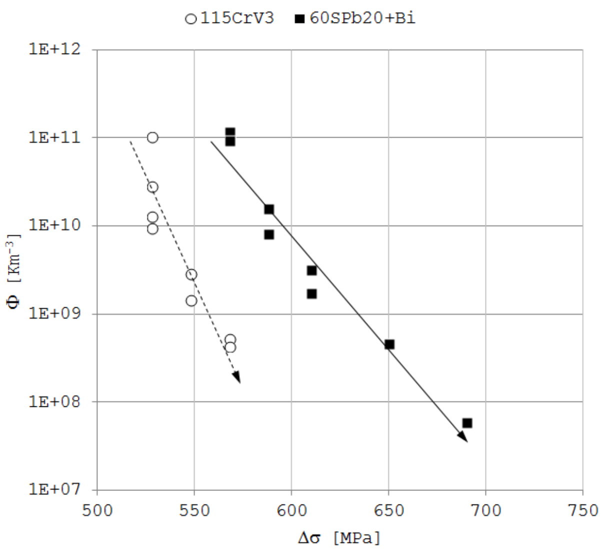

Figure 5: Integral Φ as a function of $\Delta\sigma$.

Failure Analysis

For 115CrV3 steel, the thermal treatment made by the supplier produces a spheroidized structure, as evaluated by metallographic analyses. Rockwell C hardness tests were carried out on some specimens after the fatigue tests and are reported in Tab. 2. Spheroidite can be considered a soft phase [25], thus the measured hardness values can be referred to a microstructure transformation occurred during the fatigue test.

Specimen	1	2	3
HRC	25.1	22.8	22.2

Table 2: Average Rockwell C hardness values for some 115CrV3 specimens.

Fracture surfaces of the investigated steel were observed after fatigue tests by SEM and stereomicroscope. For 115CrV3 steel, in the VHCF regime, the nucleation site of the crack is located sub-superficially at an average distance of about 100 μm from the external face. If we consider that a new phase has behaviour similar to an inclusion, its presence or a discontinuity in microstructure [26] at the initiation site is crucial for fatigue life. The microstructural transformation can have produced bainite, as confirmed by the calculated hardness and by the thermal history recorded during the test with temperatures below approximately 350 or 400 °C. The lower bainite phase [27] can be the cause of no ODA observed on the fracture surface [28, 29].

In very high cycle regime (beyond 10^7 cycles), for Pb-added steel, the initiation sites were always found at inclusions located in the interior of the specimens. Fig. 6 shows optical micrographs of the fracture surfaces. If we analyse carefully the center of the fish-eye, it is possible to find for many specimens a darker area around an inclusion, which is also the site of crack nucleation. This area is called the ODA (optically dark area). It is interesting to underline that no ODA is observed in the case of fractured specimens in the LCF regime (Fig. 6d). For the analysed specimens in the Fig. 6a and b, in the left column are reported the values of the areas of the inclusion (origin of the crack), of the so-called GBF (granular bright facet on the stage of crack propagation) and of the whole fish-eye.

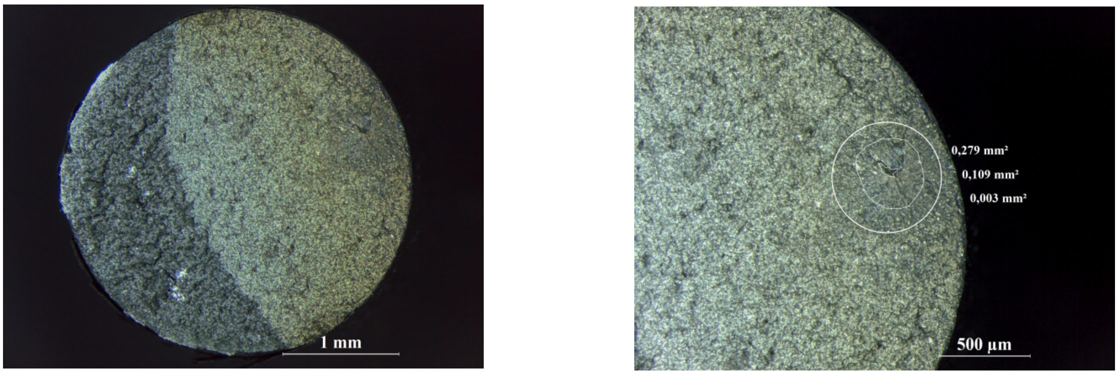

(a) M= 32X; $\Delta\sigma$= 568 MPa, N_f= $3.3\cdot10^8$ cycles. M= 50X

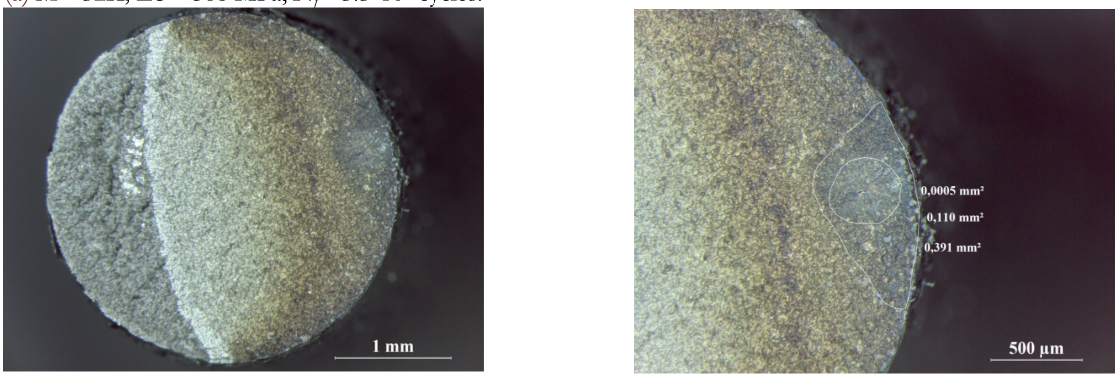

(b) M= 32X; $\Delta\sigma$= 610 MPa, N_f= $7.6\cdot10^6$ cycles. M= 50X

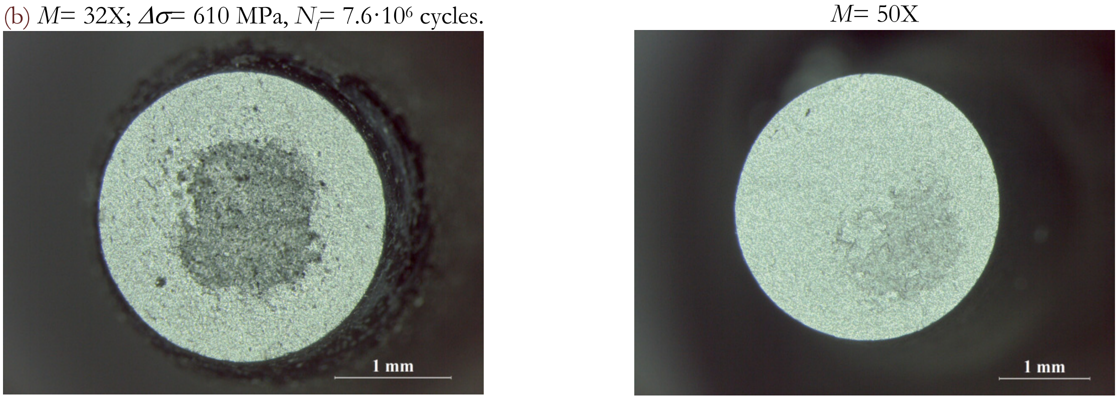

(c) M= 32X; $\Delta\sigma$= 650 MPa, N_f= $1.1\cdot10^6$ cycles. (d) M= 25X; $\Delta\sigma$= 690 MPa, N_f= $1.3\cdot10^5$ cycles.

Figure 6: Fracture surfaces of some tested specimens.

The observations at the stereomicroscope show that the GBF is more evident for the specimens that have a fatigue life over 10^6 cycles [30] and for which the area of the fish-eye increases with the fatigue life. A schematic representation of the 3 areas is shown in Fig. 7.

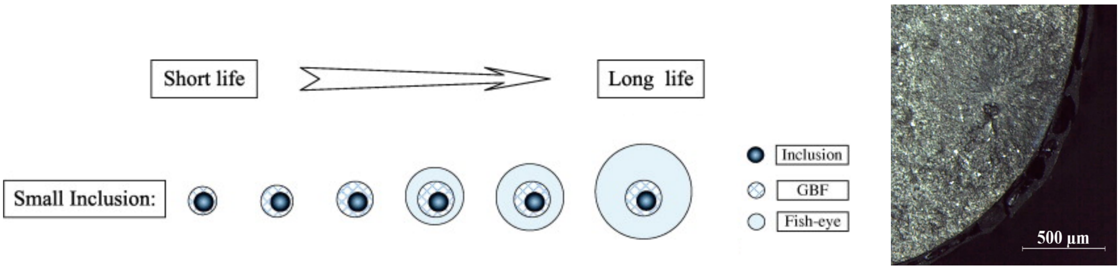

Figure 7: (a) Scheme of the fracture surface morphology [30]; (b) fish-eye particular of the specimen tested at $\Delta\sigma$ = 568 MPa and failed at N_f= 4.1·10^8 cycles.

On the other hand, fatigue initiation occurred as in a sub-surface site as on the surface. As detected by Bathias and Paris [31], the investigated Pb-added steel, for which there are no similar studies in the literature, shows a morphology of the fracture surface analogous to what is schematically reported in the Fig. 8.

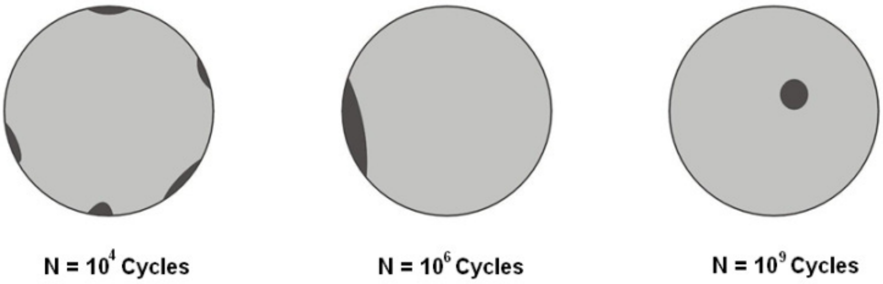

Figure 8: Scheme of the fracture surface morphology related to the fatigue endurance [31].

CONCLUSIONS

With the increasing progress of the technological development in structural applications of tool steels, the required fatigue life has increased, so it is very important to determine a safe fatigue strength for 10^9 cycles. In this paper, the behaviour of two kinds of tool steel was investigated in VHCF regime. The fatigue tests were carried out at the f = 20 kHz and R = -1 by means of an ultrasonic fatigue testing equipment. The radiometric surface temperature was detected during the whole test by means of an IR camera. The traditional Energetic Approach was developed in order to extend it in VHCF regime. The failure analysis, based on experimental techniques (scanning electron microscopy, Energy Dispersive X-ray spectroscopy and Optical Microscopy), allowed the authors to assess that the microstructure of the analysed steels influences the crack initiation and its behaviour in the VHCF regime.

NOMENCLATURE

f = frequency [Hz]
E_C = energy to failure per unit volume [Jm^{-3}]
N = number of cycles
N_{as} = asymptotic number of cycles
N_f= = number of cycles to failure
R = stress ratio
ΔT_{as} = asymptotic temperature increment during fatigue test [K]
ΔT_d = surface temperature increment during fatigue test [K]
$\Delta\sigma$ = stress range [MPa]
$\Delta\sigma_0$ = fatigue limit [MPa]
Φ = thermal increment to failure per unit volume [Km^{-3}]

REFERENCES

[1] Bathias, C., There is no infinite fatigue life in metallic materials, Fatigue Fract. Engng. Mater. Struct., 22 (1999) 559-565.
[2] Sonsino, C.M., Course of SN-curves especially in the high-cycle fatigue regime with regard to component design and safety, Int. J. Fatigue, 29 (2007) 2246-2258.
[3] Murakami, Y., Nomoto, T., Ueda, T., Factors influencing the mechanism of superlong fatigue failure in steels, Fatigue Fract. Engng. Mater. Struct. 22 (1999) 581-590.
[4] Bayraktar, E., Garcias, I.M., Bathias, C., Failure mechanisms of automotive metallic alloys in very high cycle fatigue range, Int. J. Fatigue 28 (2006) 1590–1602.
[5] Sohar, C.R., Betzar-Kotas, A., Gierl, C. et al., Fractographic evaluation of gigacycle fatigue crack nucleation and propagation of a high Cr alloyed cold work tool steel, Int. J. Fatigue 30 (2008) 2191–2199.
[6] La Rosa, G., Risitano, A., Thermographic methodology for rapid determination of the fatigue limit of materials and mechanical components, Int. J. Fatigue, 22 (2000) 65–73.
[7] Amiri, M., Khonsari, M.M., Rapid determination of fatigue failure based on temperature evolution: Fully reversed bending load, Int. J. Fatigue, 32 (2010) 382–389.
[8] Meneghetti, G., Ricotta, M., Atzori, B., A synthesis of the push-pull fatigue behaviour of plain and notched stainless steel specimens by using the specific heat loss, Fatigue Fract. Engng. Mater. Struct., 36 (2013) 1306-1322.
[9] Curà, F., Curti, G., Sesana, R., A new iteration method for the thermographic determination of fatigue limit in steels. Int. J. Fatigue, 27 (2005) 453-459.
[10] Fan, J.L., Guo, X.L., Wu, C.W., Zhao, Y., Guo, Q., Stress assessment and fatigue behavior evaluation of components with defects based on the finite element method and lock-in thermography, Special Issue "Fatigue Design and Analysis in Transportation Engineering", P. I. Mech. Eng. C. - J. Mech., (2014) doi:10.1177/0954406214541432.
[11] Crupi, V., Chiofalo, G., Guglielmino, E., Infrared investigations for the analysis of low cycle fatigue processes in carbon steels. P. I. Mech. Eng. C. - J. Mech., 225 (2011) 833 – 842.
[12] Xue, H., Wagner, D., Ranc, N., Bayraktar, E., Thermographic analysis in ultrasonic fatigue tests, Fatigue Fract. Engng. Mater. Struct., 29 (2006) 573-580.
[13] Blanche, A., Chrysochoos, A., Ranc, N., Favier, V., Dissipation Assessments During Dynamic Very High Cycle Fatigue Tests, Exp. Mech., (2014) DOI: 10.1007/s11340-014-9857-3.
[14] Fargione, G., Tringale, D., Guglielmino, E., Risitano, G., Fatigue characterization of mechanical components in service, Frat. Integ. Strut., 26 (2013) 143-155.
[15] Fan, J., Guo, X., Wu, C., Crupi, V., Guglielmino, E., Using Infrared Thermography in Effect Evaluation of Heat Treatments on Martensitic Steel, Exp. Techniques, (2014) doi: 10.1111/ext.12019.
[16] Crupi, V., An Unifying Approach to assess the structural strength, Int. J. Fatigue, 30 (2008) 1150-1159.
[17] Risitano, A., Risitano, G., Cumulative damage evaluation in multiple cycle fatigue tests taking into account energy parameters, Int. J. Fatigue, 48 (2013) 214-222.
[18] Crupi, V., Epasto, G., Guglielmino, E., Low-velocity impact strength of sandwich materials, J. Sandw. Struct. Mater., 13 (2011) 409 - 426.
[19] Mughrabi, H., On 'multi-stage' fatigue life diagrams and the relevant life-controlling mechanisms in ultrahigh-cycle fatigue, Fatigue Fract. Engng. Mater. Struct., 25 (2002) 755-764.
[20] Pyttel, B., Schwerdt, D., Berger, C., Very high cycle fatigue – Is there a fatigue limit?, Int. J. Fatigue, 33 (2011) 49-58.
[21] Plekhov, O.A., Palin-Luc, T., Saintier, N., Uvarov, S., Naimark, O., Fatigue crack initiation and growth in a 35CrMo4 steel investigated by infrared thermography, Fatigue Fract. Eng. M., 28 (2005) 169-178.
[22] Fargione, G., Geraci, A., La Rosa, G., Risitano, A., Rapid determination of the fatigue curve by the thermographic method, Int. J. Fatigue, 24 (2002) 11-19.
[23] Amiri, M., Khonsari, M.M., Life prediction of metals undergoing fatigue load based on temperature evolution, Mat. Sci. Eng. A - Struct., 527 (2010) 1555-1559.
[24] Williams, P., Liakat, M., Khonsari, M.M., Kabir, O.M., A thermographic method for remaining fatigue life prediction of welded joints, Materials and Design, 51 (2013) 916-923.
[25] ASM Handbook, Metals Handbook: Heat treatment, ninth ed., ASM International, Materials Park, Ohio (1981).
[26] Zhu, M.L., Xuan, F.Z., Chen, J., Influence of microstructure and microdefects on long-term fatigue behavior of a Cr-Mo-V steel, Mat. Sci. and Eng. A, 546 (2012) 90–96.
[27] ASM Handbook, Metallography and Microstructures, ASM International, Materials Park, Ohio (2004).

[28] Murakami, Y., Nomoto, T., Ueda, T., Murakami, Y., On the mechanism of fatigue failure in the superlong life regime ($N>10^7$ cycles). Part I: Influence of hydrogen trapped by inclusions, Fatigue Fract. Engng. Mater. Struct., 23 (2000) 893-902.

[29] Murakami, Y., Toriyama, T., Tsubota, K., Furumura, K., What Happens to the Fatigue Limit of Bearing Steel without Nonmetallic Inclusions?: Fatigue Strength of Electron Beam Remelted Super Clean Bearing Steel, Bearing Steels, In: the 21st Century, ASTM STP 1327, J. J. C. Hoo, W. B. Green (Eds.), American Society for Testing and Materials, Philadelphia (1998) 87–105.

[30] Li, W., Yuan, H., Sun, Z., Zhang, Z., Surface vs. interior failure behaviors in a structural steel under gigacycle fatigue: Failure analysis and life prediction", Int. J. of Fatigue, 64 (2014) 42–53.

[31] Bathias, C., Paris, P.C., Gigacycle fatigue in mechanical practice, Marcel Dekker, New York (2005).